J. Microlith., Microfab., Microsyst. 4(2), 023014 (Apr–Jun 2005)

Optimizing microfluidic ink delivery for dip pen nanolithography

Debjyoti Banerjee*
NanoInk, Inc.
Microfabrication Group
Campbell, California 95008

Nabil A. Amro
Sandeep Disawal
NanoInk, Inc.
Corporate Office
Chicago, Illinois 60607

Joe Fragala
NanoInk Inc.
Microfabrication Group
Campbell, California 95008

Abstract. In Dip Pen Nanolithography™ (DPN™) ultrasharp tips coated with chemical compounds (or "ink") are in contact with a surface to produce submicron sized features. There is a need to deliver multiple inks to an array of closely spaced tips (or "pens"). This work demonstrates the design optimization, fabrication process development, process optimization, and testing of a microfluidic ink delivery apparatus (called "inkwells") for simultaneously coating an array of DPN pens with single or multiple inks. The objective of this work is to deliver between four and ten different inks from reservoirs into an appropriately spaced microwell array. The tips of the multipen array are coated with the same or different inks by dipping them into the microwell array. The reservoirs, microwells, and their connecting microchannels were etched in silicon wafers using deep reactive ion etching. Fluid actuation was achieved by capillary flow (wicking). The optimum layouts for different applications were selected with respect to the volume requirement of different inks, the efficacy of ink-well filling, prevention of bubble formation, and the ease of operation (such as dipping and writing) with a parallel array of pens. [DOI: 10.1117/1.1898245]

Subject terms: dip pen nanolithography (DPN), deep reactive ion etching (DRIE), reactive ion etching (RIE), volume-of-fluids (VOF) method, microfluidics, lab-on-a-chip, capillary flow, scanning probe lithography.

Paper 04004 received Feb. 4, 2004; revised manuscript received May 25, 2004; accepted for publication Nov. 22, 2004. This paper is a revision of a paper presented at the SPIE conference on microfluidics, BioMEMS, and Medical Microsystems II, Jan. 2004, San Jose, California. The paper presented there appears (unrefereed) in SPIE Proceedings Vol. 5345; published online Apr. 22, 2005.

1 Introduction

The Dip Pen Nanolithography™ (or DPN™) process uses scanning probe tips (the "pen") coated with chemicals ("ink") to directly deposit materials with nanometer precision onto a substrate ("paper").[1] Under ambient conditions, the DPN process (Figs. 1 and 2) can deposit a variety of inorganic, organic, and biological molecules onto a variety of substrate types.[2] When using oligomer or protein-based inks, the DPN method can produce nanoscale spotted features which are much smaller than those observed in bioarrays[3] fabricated by other methods.

The objective of this work is to enable parallel writing of multiple patterns using the DPN process. An NSCRIPTOR™ system integrated with an array of pens was developed to simultaneously write multiple patterns with different inks. This requires selective deposition (i.e., coating) of ink chemistries onto the individual pens. This is accomplished by "dipping" the multipen array into "Inkwells™." The device was designed to deliver between four aqueous inks (for genomics applications) and ten aqueous inks (for proteomics applications) into an appropriately spaced inkwell array. Fluid actuation occurs by open-channel capillary flow (wicking) in microchannels, which distribute liquid from reservoirs into a microchannel and ultimately to an array of terminal microwells connected by tributaries from the microchannel (Figs. 3 and 4). Due to the large range of length scales of the layout drawings in Figs. 3 and 4 the microwells are not visible. The end of the tributary microchannels communicate with a set of microwells which range from 5 to 10 μm in diameter. Satellite reservoirs are incorporated in some of the layouts to serve as secondary sites of liquid storage and also for trapping bubbles in the flow.

2 Analysis

To understand the ink delivery it was necessary to calculate the filling times of microchannels of different sizes and the meniscus division from microchannels into tributaries. The flow rates in the microchannels were calculated from a balance of the capillary and viscous forces (and neglecting inertial forces):

$$\Delta p = \frac{4\sigma \cos\theta}{D_h} = \frac{1}{2}\rho u^2 f \frac{L}{D_h}, \tag{1}$$

where p is the pressure drop, σ is the coefficient of surface tension, θ is the contact angle, D_h is the hydraulic diameter of the channel (where $D_h = 4A/P_w$, A is the cross-sectional area for flow direction and P_w is the wetted perimeter of the cross section), ρ is the density of liquid flowing in the microchannels, u is the average velocity in the microchannels, f is the Darcy-Weisbach friction factor,[4,5] and L is the

*Current address: Department of Mechanical Engineering, Texas A&M University, College Station, TX 77843-3123.
1537-1646/2005/$22.00

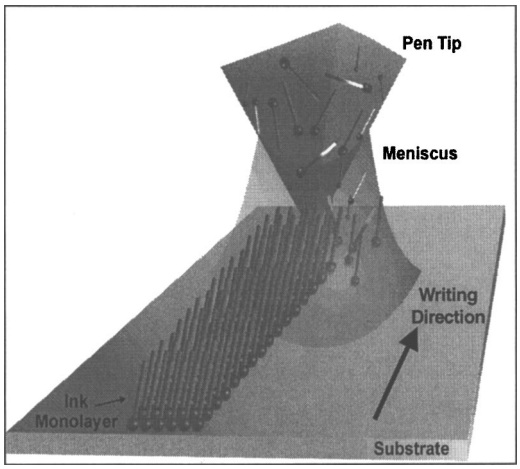

Fig. 1 Diagram illustrating the principle of dip pen nanolithography (DPN).

length of the channel. For laminar flow in circular channels, $f=64/\mathrm{Re}_{D_h}$, where $\mathrm{Re}_{D_h}=\rho u D_h/\mu$, where Re_{D_h} is the Reynolds number and μ is the kinematic viscosity of the working liquid. For rectangular channels, the friction coefficient is from -11% to $+40\%$ of the value for circular channels, depending on the aspect ratio, where the aspect ratio =height/width. For example, for a rectangular channel of aspect ratio 10, the friction factor is given by $f=84.68/\mathrm{Re}_{D_h}$, which is 30% higher than for a circular cross section. For a square cross section (aspect ratio=1), the friction factor is given by $f=56.91/\mathrm{Re}_{D_h}$, which is 11% lower than for a circular cross section. Other values of friction factor can be obtained for different aspect ratios in many standard introductory text books on thermofluidics.[4,5]

Using the formulation for f (valid for $\mathrm{Re}_{D_h}<2000$) for a circular cross section, Eq. (1) can be simplified as

$$uL=D_h\sigma\cos\theta/8\mu. \tag{2}$$

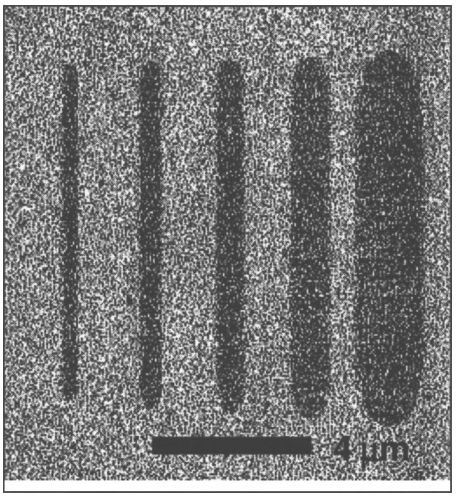

Fig. 2 DPN method-generated patterns of 16-mercaptohexadecanoic acid (MHA) on gold.

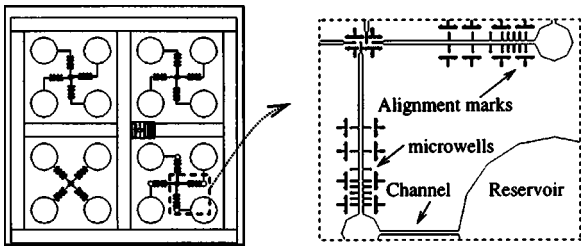

Fig. 3 Mask layout showing four different layouts for delivery of four different inks. The inset shows the location of reservoirs (diameter: 1 mm), satellite reservoirs, microchannel, alignment marks, microwells, and tributaries connecting the microchannels. The microwell are located at the end of the tributaries and are not clearly visible due to the large range of length scales in the layout.

Using properties of water, the initial velocity of fluid flow in the microchannels can be calculated to be of the order of 1 m/s for $L/D_h>10$. This estimate matched very well with experimental data described later. Equation (2) can be used to estimate the filling time (τ) as

$$\tau=\int_{L_1}^{L_2}\partial L/u=\frac{1}{2}(L_2^2-L_1^2)\frac{8\mu}{D_h\sigma\cos\theta}. \tag{3}$$

Equation (3) can be written in nondimensional form as

$$\left[\frac{\sigma\cos\theta/D_h}{4\mu}\right]\tau=\frac{L_2^2-L_1^2}{D_h^2}. \tag{4}$$

For rectangular channels (of aspect ratio 10) the coefficient on the denominator of the left-hand side of Eq. (4) would be 5.3 (instead of 4), which is about 30% higher. Equation (3) is used to calculate the filling time of microchannels of different hydraulic diameters using the following thermophysical properties: $\mu=10^{-5}$ kg/m s, $\sigma=0.07$ N/m, and $\theta=20°$. The results of the calculation are plotted in Fig. 5. As mentioned before, the time required for filling rectangular channels of aspect ratio 10 would be 30% higher than the values plotted in Fig. 5. The results show that for the same length the wider channels (larger D_h) fill up faster than the narrow channels. This is due to capillary forces ($\sim 1/D_h$) being retarded by even larger pressure drop ($\sim D_h^2$) in narrow microchannels. The time calculated by the previous analyses would overpredict the filling time of the microchannels by less than 1% if inertia effects are

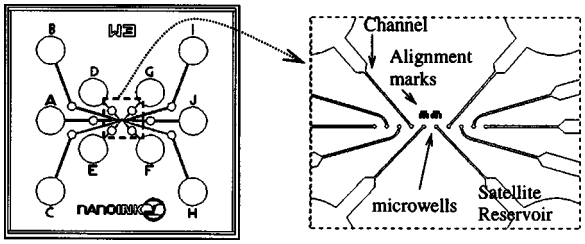

Fig. 4 Mask layout showing a different layout for delivery of ten different inks. The inset shows the location of reservoirs (diameter: 1 mm), satellite reservoirs, microchannel, alignment marks, microwells, and tributaries connecting the microchannels.

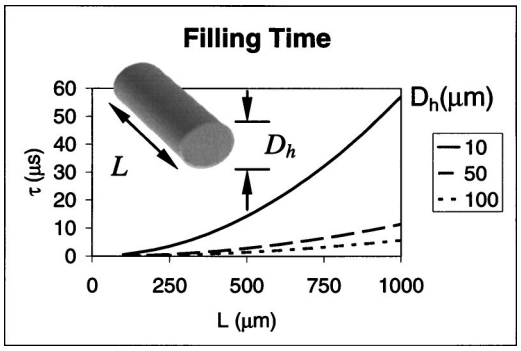

Fig. 5 Filling time (τ) in microseconds for capillary flow of water in microchannels of different length (L) and hydraulic diameter (D_h) using Eq. (3).

included (for $L/D_h > 10$). The error in the estimated fill time is thus less than 1%. The analysis also shows that filling time is lower for open-channel flow (D_h is lower) than for pipe flow.

The analyses for microchannel (and microwell) filling is important for ensuring reliability of the device. The exercise of calculating the filling speed also gives insight into the order by which the tributary microchannels and microwells are filled. The filling process is slower in the tributary microchannels due to the higher flow pressure drop required in channels with lower hydraulic diameter, D_h. Such an approach ensures that the main microchannel is filled first before the tributaries for certain dimensions of the main microchannel and the tributaries. The employed design principle ensures uniform distribution and filling of the microwells. This strategy reduces susceptibility to bubble formation in the tributary microchannels and therefore ensures better reliability of the device.

3 Computational Fluid Dynamics Simulation

The volume of fluids (VOF) method was used to verify the analysis mentioned previously. Also, a design choice to use closed-channel flow (or ''pipe flow'') or open-channel flow was made based on the computational fluid dynamics (CFD) simulation results. The models were created and tested using the VOF method in the CFD-ACE+ design and simulation multiphysics software (CFD Research Corporation, Hunstville, AL). In open-channel flow, there is less susceptibility to bubble formation for liquid flow in the microchannels and during the filling of the microwells. However, the trade-off for this design is the enhanced evaporative loss of the inks, especially for liquids with high vapor pressure under ambient conditions. The evaporative losses in closed-channel (or pipe flow) are lower—however, the microwells, microchannels, and reservoirs have a greater propensity to form bubbles during filling. Bubble formation in these components can impede capillary flow and can lead to catastrophic failure for fluid actuation in these devices. It was verified from the simulations that the filling time is lower in the open channel than pipe flow and is consistent with the analytical results.

Figures 6 and 7 shows a simulation of meniscus breakup from a 5-μm-wide channel into a 2-μm-wide tributary (both 10 μm deep) using the VOF method. The simulations were performed for thermofluidic property values of water

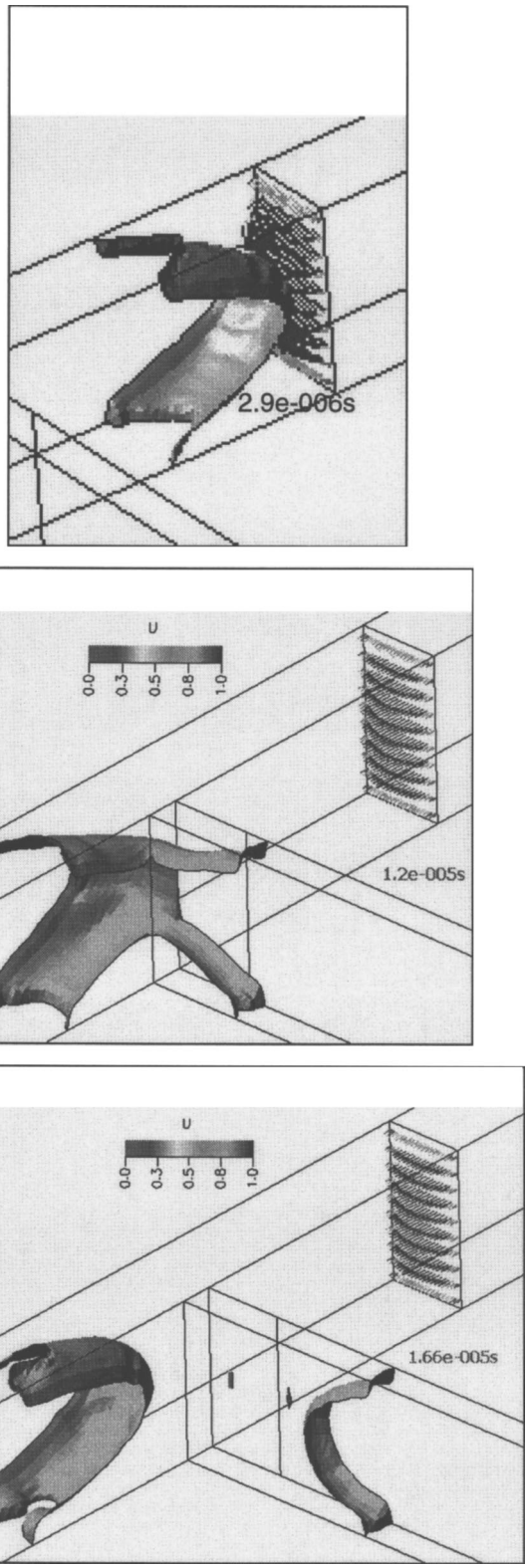

Fig. 6 Temporal simulation of meniscus shapes for microchannel filling in pipe flow.

at room temperature (where $T=298$ K, $\rho=996.5$ kg/m^3, $\mu=10^{-3}$ kg/m s, $\sigma=0.07$ N/m, and $\theta=20°$). For pipe flow simulations, the boundary conditions imposed were: wall boundary conditions on the sides, outlet boundary condition

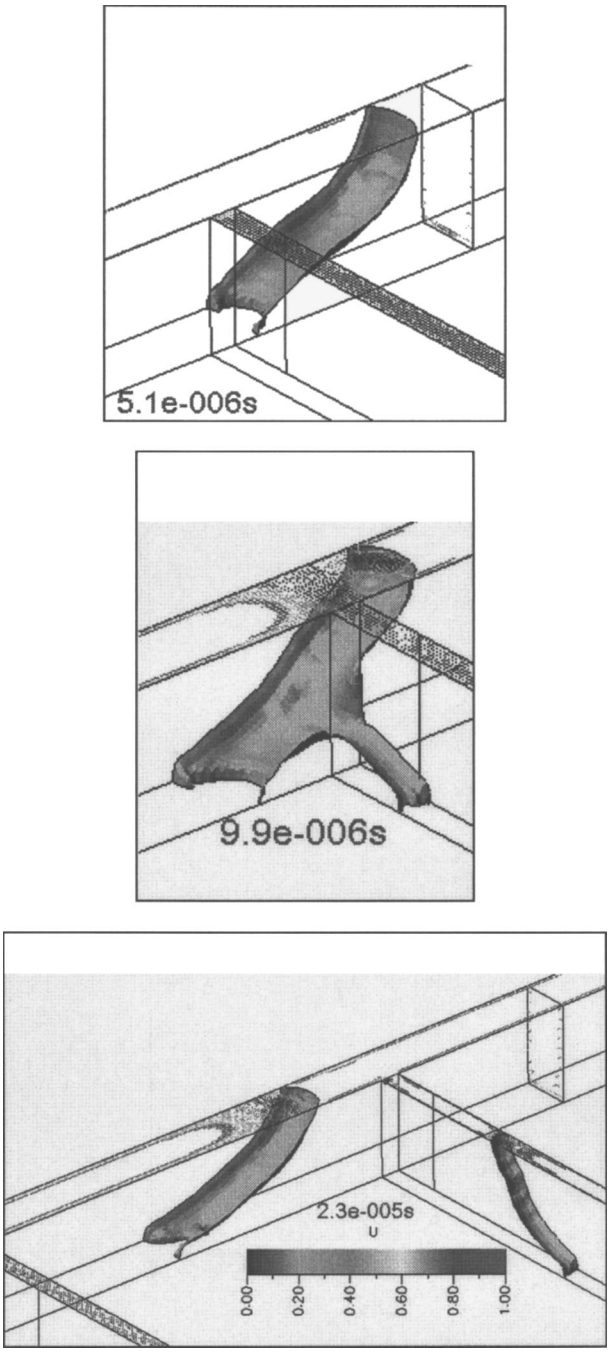

Fig. 7 Temporal simulation of meniscus shapes for filling in open-channel flow.

at the end of the channels, and inlet boundary condition at the beginning of the channel flow region. For open-channel flow simulations, the boundary conditions imposed were: wall boundary conditions on the sides, outlet boundary condition at the end of the channels, outlet boundary conditions on the top surface, and inlet boundary condition at the beginning of the channel flow region. For both set of simulations, a fluid initial condition was imposed with a stationary volume of liquid, which was 40 μm long from the inlet region.

The sequence of images in Fig. 6 obtained from CFD simulations shows that the meniscus breakup process is initiated at the top and bottom wall in pipe flow. The sequence of images in Fig. 7 obtained from CFD simulations shows that the meniscus breakup process is initiated at the bottom wall for open-channel flow and therefore has less susceptibility to trap bubbles during the filling process.

The simulation data also validate the analytical prediction that the filling process is faster in the wider channel compared to the narrower tributary channel. By measuring the time of travel of the meniscus in the wider microchannel (before meniscus bifurcation and flow distribution into the smaller tributary microchannels) the speed of the meniscus movement was found to be of the order of 1 m/s. This is consistent with results from Eq. (3) for $L/D_h > 10$ and using the thermophysical property values of water mentioned previously. The numerical results showed that there is a reduction in the velocity of the meniscus when the flow is distributed from the wider microchannel into the tributaries. This is expected due to a higher pressure drop that occurs on the distribution of the flow into more than one microchannel compared to the enhanced capillary pressure arising from meniscus bifurcation into more than one microchannel. The results from the CFD simulation were used to select, design, and optimize the layout of the inkwells for using open-channel capillary flow configuration.

4 Fabrication

Different wet and dry etching methods were investigated. Figure 8(A) demonstrates the initial process flow for fabricating the inkwells using reactive ion etching (RIE). In this process, a $\langle 100 \rangle$ silicon wafer was oxidized in a Thermco Minibrute oxidation furnace for 4 h to obtain an oxide layer thickness of approximately 1 μm. Photoresist was patterned on the oxidized silicon wafer and the underlying silicon substrate was exposed by using a timed wet etch of the oxide layer in HF solution. A Technic RIE was then used to etch the microfluidic components in the silicon substrate. The inkwells were limited to a depth of 10 μm when fabricated using this process flow, due to etching constraints of the RIE process.

Due to rapid evaporative loss of aqueous inks these inkwells could only be used for less than a minute from the point of loading to the point of complete evaporative loss of the inks. Also, there was no mechanism for controlling cross contamination between different inks used in adjacent microwells. It was decided that high aspect ratio (10:1) microfluidic structures were needed to maximize the retention time of the inks in the inkwells. Also, hydrophobic barriers were designed to contain the inks in their respective microwells and prevent cross contamination. Deep reactive ion etching (DRIE) using the Bosch process (STS Limited, Imperial Park, Newport, UK) was found to be the most suitable method [Fig. 8(B)] for etching the high aspect ratio microfluidic features.

In this optimized process flow, a layer of hydrophobic fluoro-polymer (order of 100 nm) was first deposited on a silicon wafer using a polymer passivation step typically used in DRIE process cycles. Photoresist was patterned on the polymer coated silicon wafer. The patterned photoresist was used to selectively etch the polymer layer and the silicon substrate by the Bosch process to form the microfluidic components (channels, microwells, and reservoirs). The remaining photoresist was stripped off and the wafer was

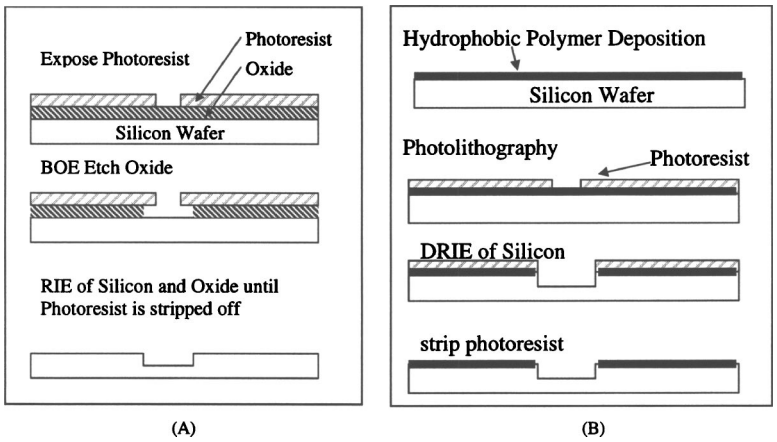

Fig. 8 Process flow diagrams.

cleaned in a piranha bath (mixture of sulphuric acid and hydrogen peroxide, 3:1 ratio by volume). The hydrophobic polymer, which was selectively deposited and patterned on the top surface of the wafer, forms the barriers for controlling cross contamination. The high aspect ratio vertical sidewalls in the microfluidic devices coupled with hydrophobic barriers enabled the retention time of the aqueous inks in the inkwells to be increased to more than 10 min. Figure 9 shows the scanning electron microscopy (SEM) images of different inkwell layouts obtained by using the optimized process flow.

5 Experimental Apparatus

Nanoliter volume droplets were deposited into the reservoirs using a syringe with a microneedle (Hamilton Company, Reno, NV) and Model P-10 3-axis micropositioner with an inker bracket (Miller Design, San Jose, CA) for filling the reservoirs. The movements of the menisci in the microchannels were recorded using an imaging apparatus, comprising of a high resolution Pulnix-TM1300 camera (1300×1030 pixels), a Road Runner R12 frame grabber, Nikon-SMZ10A trinocular microscope (with ring illumination) and PC for data acquisition. Image Pro Express software (Media Cybernetics, Silver Spring, MD) was used for image analysis. Figure 10 shows the apparatus for loading the inkwells and recording the images for microwell filling.

6 Results and Discussion

The inkwells were loaded with various types of inks and their efficacy was tested for filling, dipping of pens, and writing. Figure 11 shows temporal sequence images of meniscus movement from a reservoir into the array of inkwells after loading the reservoir with ink. The reservoirs in these images were loaded with a solution of 40% ethylene glycol in water. From the sequence of images it was estimated that the speed of meniscus movement in the microchannels

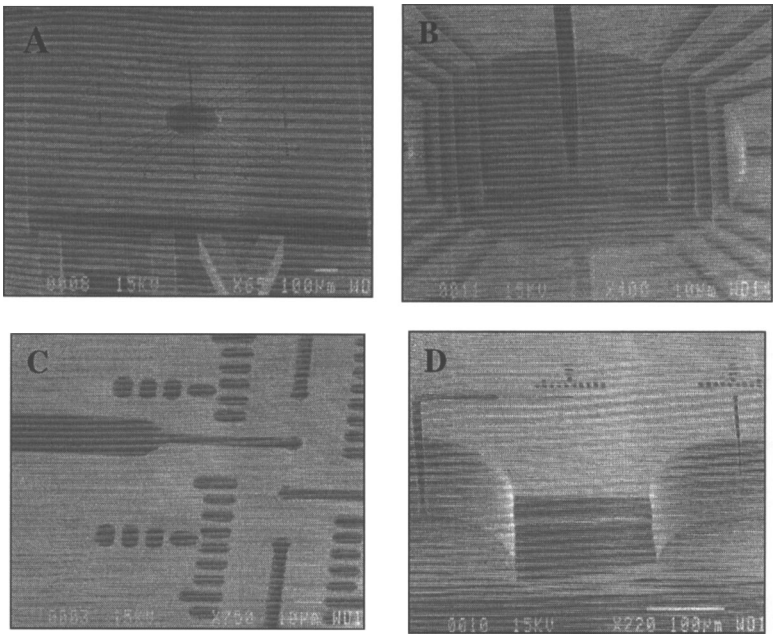

Fig. 9 SEM images of inkwells. (A) Overview of reservoir and microwells, (B) close-up view of reservoir, (C) close-up view of microwells with alignment marks, and (D) cross-section of reservoir and microchannel.

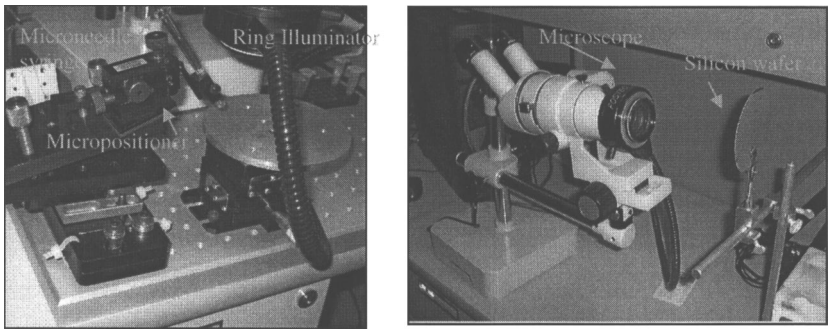

Fig. 10 Apparatus for loading inkwells and viewing the filling process.

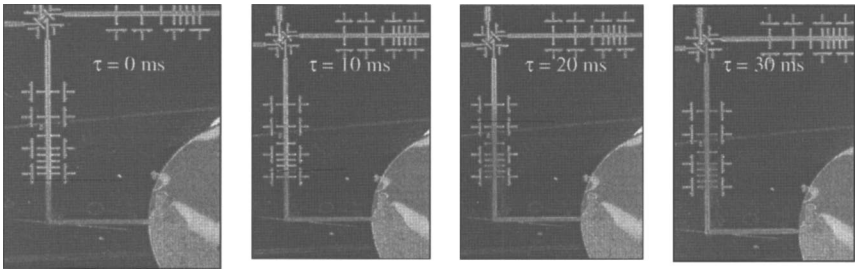

Fig. 11 Time sequence images of meniscus motion in microchannel from reservoir to microwells. For purposes of clarity, the location of the meniscus in each frame has been indicated by a dashed line (except the last frame, where the microchannels are completely filled).

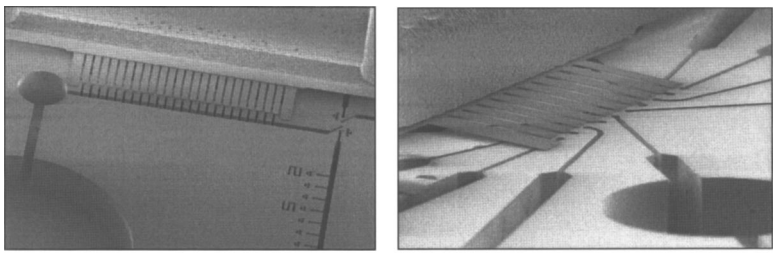

Fig. 12 SEM images showing DPN pens aligned with microwells in inkwells (courtesy of Dr. Bjoern Rosner, NanoInk, Inc.).

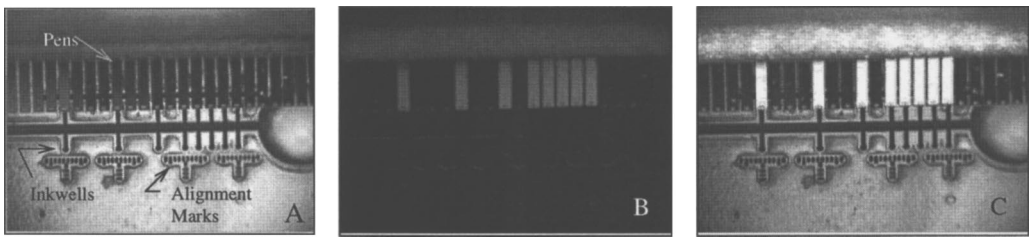

Fig. 13 (A) A multipen array is aligned with an array of microwells (light on), (B) tips are dipped into the microwells (light off), and (C) illuminated image showing dipped pens reflecting light differently than the undipped pens.

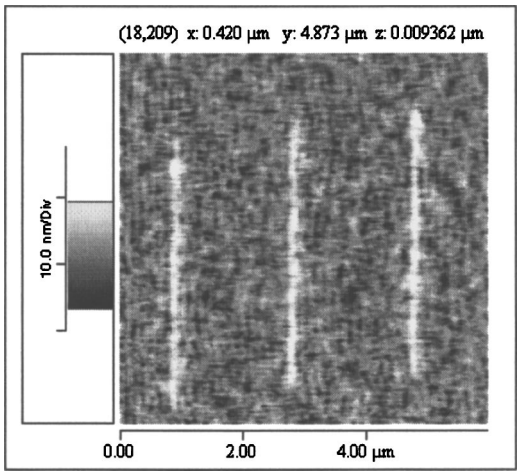

Fig. 14 Lateral force microscopy (LFM) image of patterns written on a glass substrate using DPN pen dipped in a solution of 40% ethylene glycol in water. The three straight lines were written using a pen array consisting of three tips which were dipped simultaneously in three separate microwells.

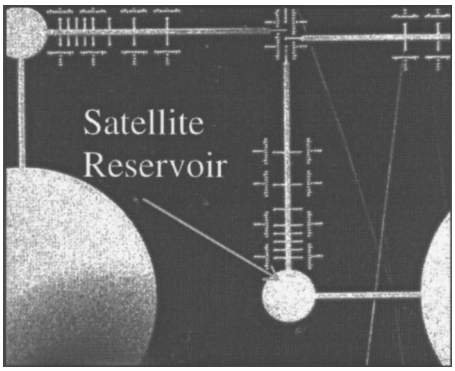

Fig. 15 Optimal design selected from this study incorporating a satellite reservoir as a bubble trap.

reached 1 m/s before the filling of the microwells or the tributaries. This is consistent with the analytical calculations and the CFD simulation data for thermophyscial properties of water (mentioned before in Sec. 3).

Figure 12 shows SEM images of two different DPN pen arrays aligned with microwells in two different inkwells. Figure 12(A) shows a 24-tip pen array dipped into microwells in a manner that would coat all the pens with the same ink. Figure 12(B) shows a 10-tip pen array into microwells that could coat each pen with a different ink.

Figure 13 shows a set of images obtained from a dipping experiment. The images depict the alignment of the multipen array and the dipping of the pens into the inkwells filled with ethylene glycol solution. In the images, the dipped pens are pulled into their respective microwells by capillary action. The resulting deflection of the corresponding cantilevers is observed as a change in the intensity of light reflected from the dipped cantilevers. The dipped pens were used to write nanoscale patterns on a glass surface using DPNWrite™ instrument software. The written patterns were imaged using an M5 atomic force microscope (Park Scientific, currently part of Veeco Instruments, Santa Barbara, CA). Figure 14 shows a lateral force microscopy image of a written pattern. Three different lines were written simultaneously by a three-pen array. The three pens were uniquely coated with hydrophilic ink by dipping them into microwells in an inkwell chip loaded with 40% ethylene glycol in water. The choice of an ethylene glycol mixture as the ink material was made after observing the high rate of evaporation of pure water.

Rapid evaporation of some inks such as mercaptohexadecanoic acid (MHA) in acetonitrile or ethanol is a time-limiting factor for using in inkwells. A water-based ink was found to remain usable for at least 10 min in ambient conditions before evaporation depleted the inkwells. High boiling point inks such as ethylene glycol–water mixture was found to stay in the microwells for few hours. A representative DPN experiment is shown in Fig. 14. We found alcohol-based inks (hexanol, heptanol, octanol, etc.) with high boiling points (above 150 °C) result in evaporation time between 30 min and 6 h in the inkwells. Figure 16 shows an example of a successful writing operation using MHA in octanol as a hydrophobic ink. First a bitmap image is converted using InkMap™ routine in the InkCad™ software to a DPN version, as shown in Fig. 16(A). Figure 16(B) shows a miniature pattern of the converted bitmap image consisting of an array of dots and printed using DPN with MHA ink on gold. Pens inked in inkwells filled with MHA–octanol show nearly the same ink diffusion coefficient as manually coated probes.

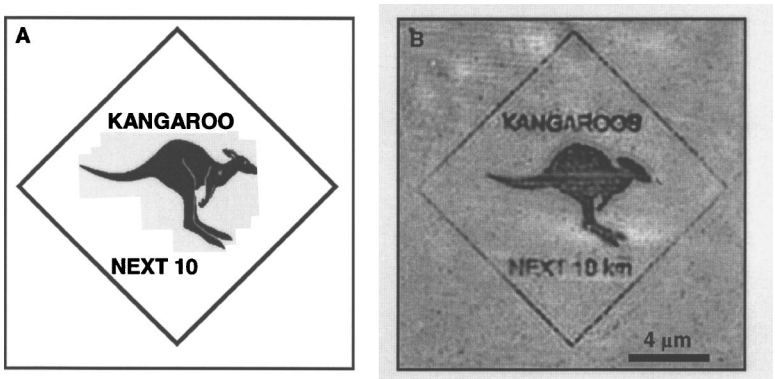

Fig. 16 MHA ink used in inkwells. (A) A bitmap pattern prior to being converted as a pattern for DPN using InkMap™ and (B) AFM lateral force image of a pattern written with a probe inked in inkwells filled with MHA octanol which displays high quality writing.

From the experiments it was found that the designs incorporating a satellite reservoir (which also serves as a bubble trap) had the most desirable characteristics for inkwell filling, dipping and writing (Figs. 4 and 15). Other layouts developed in this investigation (shown in Fig. 3) were found to be deficient in filling efficacy, processing sensitivity, reliability (bubble formation and bubble trapping) or ease of dipping a pen array.

7 Conclusion

Design optimization and process optimization were performed to fabricate the optimal microwell layout for using four and ten different inks to perform DPN using multipen arrays. The ink coated pens were successfully used to simultaneously write multiple patterns on a glass surface. A satellite reservoir was incorporated in the optimized layout to serve as a secondary storage for the working liquid and also to successfully trap bubbles in the flow (and enhance the reliability of the inkwell device).

Acknowledgments

The authors are grateful to the MEMS Team, Chemistry Team, and the Instrumentation Team. The authors would like to thank Dr. Bjoern Rosner, Dr. Robert Elghanian, and Dr. Ray Eby at NanoInk Inc. for their help with this work. This work would not have been possible without the previous and continuing DPN research and MEMS development efforts of the Mirkin research group at Northwestern University and the group of Chang Liu at the University of Illinois at Urbana–Champaign. DPN™, Dip Pen Nanolithography™ and Inkwell™ are trademarks or registered trademarks of NanoInk Inc.

References

1. R. D. Piner, J. Zhu, F. Xu, S. Hong, and C. A. Mirkin, ''Dip-pen nanolithography,'' *Science* **283**, 661–663 (1999).
2. L. M. Demers, D. S. Ginger, S.-J. Park, Z. Li, S. W. Chung, and C. A. Mirkin, ''Direct patterning of DNA on metal and insulating substrates via dip-pen nanolithography,'' *Science* **298**, 1836–1838 (2002).
3. A. D. Barone, J. E. Beecher, P. A. Bury, C. Chen, T. Doede, J. A. Fidanza, and G. McGall, ''Photolithographic synthesis of high-density oligonucleotide probe arrays,'' *Nucleosides, Nucleotides & Nucleic Acids* **20**(4–7), 525–531 (2001).
4. F. M. White, *Fluid Mechanics*, 3rd ed., McGraw-Hill, New York (1994).
5. A. F. Mills, *Heat and Mass Transfer*, Irwin (1995).

Debjyoti Banerjee received his PhD from UCLA in mechanical engineering with major in heat and mass transfer and minor in MEMS and fluid mechanics. His PhD research work was published in the Journal of Heat Transfer and received the ''2001 Best Journal Paper Award'' from the ASME Heat Transfer Division. He has received three MS degrees and was invited to the membership of four national academic honor societies. He attended the University of Mississippi for his MS degrees and Indian Institute of Technology (I.I.T.), Kharagpur for his bachelor of technology (honors) degree. Prior to joining NanoInk Inc. he worked at Tata Iron & Steel Co., Coventor Inc. and Ciphergen Biosystems Inc. Most recently he was the Manager of Fluidics and Device Engineering in the Advanced Research and Technology group at Applied Biosystems Inc. Presently he is at the Texas A&M University as assistant professor of mechanical engineering. His research interests are in thermofluidics (multiphase flow, boiling), microfluidics, MEMS, and nanotechnology.

Nabil A. Amro got his PhD degree in chemistry from University of California at Davis majoring in physical chemistry on the subject of ''high-resolution imaging and nanofabrication of biosystems from ligands, proteins to bacteria'' under the supervision of Professor Gang-yu Liu. He has been a receiver of NSF-IGERT fellowship from 1998 to 2002 during his PhD work. His research was published in peer-reviewed scientific journals. He specializes in scanning probe microscopy and its application in nanotechnology. He also attended Western Michigan University for his master degree and Lebanese University Faculty of Sciences for his bachelor degree. He joined NanoInk, Inc. in 2003 as its second chemist and nanotechnologist. He is currently working on the design of advanced nanolithography techniques, ink formulation and characterization and method development for dip pen nanolithography (DPN).

Sandeep Disawal earned his masters degree from Louisiana Tech University in chemical engineering with emphasis on microfabrication and nanofabrication. At LaTech, he performed research work on layer-by-layer self-assembly, under the supervision of Dr. Yuri Lvov, and used it to nanofabricate thin multilayers of polymers, proties, and nanoparticles to develop nano-bio reactors. He attended Ravi Shankar University for his Bachelor of Engineering (honors) degree. After completing his graduate degree in 2002, he has been working for Nanoink, Inc. as a chemical engineer. His research interest revolves around nanofabrication techniques, process development and optimization.

Joe Fragala is NanoInk's Vice President of Microfabrication and MEMS where he brings over 20 years of semiconductor and MEMS experience. Prior to joining NanoInk, he served as Endevco's general manager of their silicon sensor production plant leading both the development of new products and the production of over 60 different MEMS sensors—including pressure sensors, angular rate sensors, and accelerometers. Previously, he worked at JPL/NASA as a member of the technical staff designing and fabricating a high-performance tunneling accelerometer. He also worked as program manager of Kavlico Corporation (a Solectron Company), fabrication manager for Silicon Detector Corp., and R&D engineer at Gould Medical/Viaggo-Spectramed. He earned his BA in chemistry in 1982 from the College of the Holy Cross in Massachusetts.